Efficient Analysis of Planar Microstrip Geometries Using a Closed-Form Asymptotic Representation of the Grounded Dielectric Slab Green's Function

MIGUEL MARIN, MEMBER, IEEE, SINA BARKESHLI, AND PRABHAKAR H. PATHAK, FELLOW, IEEE

Abstract—A newly developed closed-form asymptotic representation of the grounded dielectric slab Green's function can be very efficiently applied to analyze planar microstrip configurations. In this study, such a representation is used in a moment method formulation to calculate the propagation constant of an infinite microstrip transmission line and the input impedance of a finite length, center-fed printed dipole. In these problems, source and field points are laterally rather than vertically separated with respect to the substrate. The conventional Sommerfeld integral and the plane wave spectral integral (PWS) representations of the microstrip Green's function converge very slowly in this case. However, the asymptotic closed-form representation of the Green's function does not have this limitation, and it remains accurate even for very small lateral separation between source and observation points. Only for observation points in the immediate vicinity of the source is a modified form of the Sommerfeld integral representation used, while the asymptotic form is employed elsewhere. Some numerical results based on this approach are presented and are shown to compare very well with previous results based on the corresponding exact-integral or PWS forms of the Green's function.

I. INTRODUCTION

THE INCREASING interest in monolithic microwave integrated circuit (MMIC) technology has led to the need for accurate, rigorous characterization of passive circuit and radiating elements, especially in millimeter-wave regimes. In microstrip structures, CAD tools capable of handling a wide range of dielectric constants and substrate thicknesses are required. Although "full-wave" (moment method based) analyses of some microstrip geometries have been reported recently, they involve an enormous computational effort to numerically evaluate the grounded dielectric slab Green's function, either in its plane-wave spectral (PWS) integral representation [1] or in terms of Sommerfeld-type integrals [2]. This effort has been shown to be reduced drastically by using asymptotic forms of the Sommerfeld integrals [3], [4], even valid for observation points very close to the source. The purpose of this paper is to show the application of this newly developed asymptotic closed-form approximation of the microstrip Green's function to solve some planar canonical microstrip configurations. This efficient asymptotic Green's function is specifically applied to the calculation of the propagation constant of an infinite microstrip transmission line and the input impedance of a finite-length center-fed microstrip dipole, shown in Fig. 1(a) and (b), respectively.

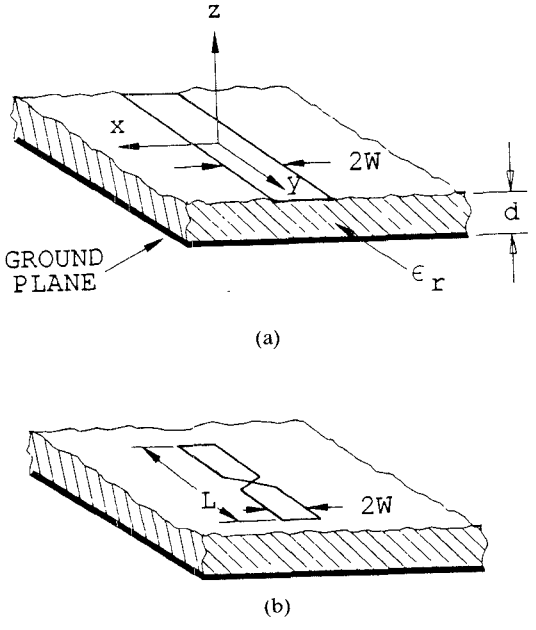

Fig. 1. Geometry of an (a) infinite microstrip line and (b) center-fed printed dipole.

The format of this paper is as follows. First, Section II deals with the conventional Sommerfeld integral representation of the grounded dielectric slab (microstrip) Green's function and its closed-form asymptotic approximation. Section III describes their application to the evaluation of the propagation constant of an infinite microstrip line, while a moment method (MM) formulation for the input

Manuscript received August 1, 1988; revised November 14, 1988. This work was supported in part by the Joint Services Electronics Program under Contract N00014-88-K-0004 and by the Ohio State University Research Foundation.

The authors are with the Ohio State University ElectroScience Laboratory, 1320 Kinnear Road, Columbus, OH 43212.

IEEE Log Number 8826034.

0018-9480/89/0400-0669$01.00 ©1989 IEEE

impedance of a center-fed microstrip dipole is presented in terms of these Green's functions in Section IV. Finally, Section V is dedicated to numerical results and conclusions.

II. The Grounded Dielectric Slab Green's Function—Conventional Integral and Asymptotic Forms

In this section, we will restrict our attention to the $\hat{y}\hat{y}$ component of the grounded dielectric slab Green's function (G_{yy}), since it will be the only one used throughout the paper. It represents the $\hat{y}$-directed electric field at (x, y) due to a $\hat{y}$-directed electric dipole of unit strength located at (x', y'). For source and observation points both lying on the surface of the slab, G_{yy} can be written in terms of the conventional Sommerfeld-type integrals as [3], [4]

$$G_{yy}(\rho) = \frac{-1}{2\pi\omega\epsilon_0}\left\{k_0^2 U + \frac{\partial^2}{\partial y^2}\left[U - \frac{\epsilon_r - 1}{\epsilon_r} W\right]\right\} \quad (1)$$

where

$$\rho = \sqrt{(x-x')^2 + (y-y')^2}$$

$$U = \int_0^\infty J_0(\xi\rho) F_u(\xi)\, d\xi \quad (2)$$

$$W = \int_0^\infty J_0(\xi_\rho) F_w(\xi)\, d\xi \quad (3)$$

and

$$F_u(\xi) = \frac{\xi}{D_e(\xi)} \quad (4)$$

$$F_w(\xi) = \frac{\sqrt{k_0^2 - \xi^2}\,\xi}{D_e(\xi)\cdot D_m(\xi)} \quad (5)$$

$$D_e(\xi) = \sqrt{k_0^2 - \xi^2} - j\sqrt{\epsilon_r k_0^2 - \xi^2}\cdot\cot\left[d\sqrt{\epsilon_r k_0^2 - \xi^2}\right] \quad (6)$$

$$D_m(\xi) = \sqrt{k_0^2 - \xi^2} + \frac{j}{\epsilon_r}\sqrt{\epsilon_r k_0^2 - \xi^2}\cdot\tan\left[d\sqrt{\epsilon_r k_0^2 - \xi^2}\right]. \quad (7)$$

In the above equations, k_0 is the free-space wavenumber, d the slab thickness, and ϵ_r the relative dielectric constant of the substrate. In the following, ϵ_r will be assumed to be a real number (lossless case). As will be shown later, the second derivative in (1) can be removed using integration by parts, so the problem of computing the Green's function reduces to one of evaluating the functions U and W. Two main problems arise in the numerical evaluation of (2) and (3). First, the integrands exhibit a certain number of poles (zeros of D_e, D_m) and, second, the slowly decaying oscillatory behavior of the Bessel function results in a poor convergence of the integrals.

A. Numerical Evaluation of U, W for ρ Small

A relatively efficient technique for evaluating U and W when ρ is small (less than one or two free-space wavelengths) is the so-called asymptotic (not to be confused with the closed-form asymptotic representation of the Green's function) extraction technique [3], [5], [6]. One first notes that the functions $F_{u,w}$ in (2) and (3) tend to certain limiting values for ξ large:

$$F_u^\infty = \lim_{\xi\to\infty} F_u(\xi) = \frac{j}{2} \quad (8)$$

$$F_w^\infty = \lim_{\xi\to\infty} F_w(\xi) = \frac{j}{2}\frac{\epsilon_r}{\epsilon_r + 1}. \quad (9)$$

Therefore, we can rewrite (2) and (3) as

$$U = F_u^\infty \int_0^\infty J_0(\xi\rho)\, d\xi + \int_0^\infty J_0(\rho\xi)\{F_u(\xi) - F_u^\infty\}\, d\xi \quad (10)$$

$$W = F_w^\infty \int_0^\infty J_0(\xi\rho)\, d\xi + \int_0^\infty J_0(\rho\xi)\{F_w(\xi) - F_w^\infty\}\, d\xi. \quad (11)$$

Since the first integral has a closed-form result and the integrand in the second becomes zero for ξ large, we can finally write the above equations as

$$U = \frac{F_u^\infty}{\rho} + \int_0^{\xi_u^\infty} J_0(\rho\xi) F_u'(\xi)\, d\xi \quad (12)$$

$$W = \frac{F_w^\infty}{\rho} + \int_0^{\xi_w^\infty} J_0(\rho\xi) F_w'(\xi)\, d\xi \quad (13)$$

where ξ_u^∞ and ξ_w^∞ are those values of ξ for which $F_u \approx F_u^\infty$ and $F_w \approx F_w^\infty$. These expressions for U and W have two important advantages over (2) and (3). First, the singularity in U and W has been explicitly extracted ($1/\rho$ term). Second, the infinite integration has been reduced to a finite interval. Typical values of $\xi_u^\infty, \xi_w^\infty$ for $\rho = 0$ (most unfavorable case) range around $5k_0\sqrt{\epsilon_r}$.

To deal with the poles of $F_{u,w}'$ in (12) and (13), one uses conventional singularity extraction techniques [3], [5]. These poles will be located on the real ξ axis for the lossless case, in the region $[k_0, k_0\sqrt{\epsilon_r}]$. Their number and location depend on the wavenumber, the dielectric constant, and the substrate thickness and can be easily found using a Newton–Raphson search algorithm with appropriate starting values [7].

The main limitation of this approach comes from the highly oscillatory behavior of the integrands in (12) and (13) for large values of ρ. This makes numerical integration very inefficient.

B. Asymptotic Closed Forms of U, W for ρ Large

Although the details of the derivation of the asymptotic representation can be found in [4], we will summarize the procedure here as follows.

First, and due to the oddness of $F_{u,w}$, integrals (2) and (3) can be written as

$$U = \frac{1}{2}\int_{C_1} F_u(\xi) H_0^{(2)}(\rho\xi)\, d\xi \quad (14)$$

$$W = \frac{1}{2}\int_{C_1} F_w(\xi) H_0^{(2)}(\rho\xi)\, d\xi \quad (15)$$

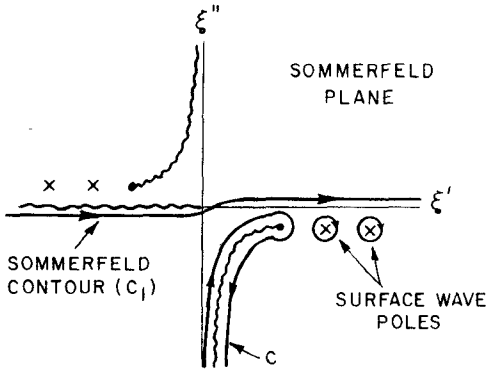

Fig. 2. Original Sommerfeld contour of integration (C_1) and its deformation to give the sum of the enclosed residues plus the integral around the branch cut (C).

where C_1 is the path shown in Fig. 2. This path C_1 can be deformed into C as shown in Fig. 2 to give the sum of the enclosed residues plus the integral around the branch cut:

$$U = -\frac{1}{2}\sum_{i} 2\pi j R_u(\xi_i) H_0^{(2)}(\rho\xi_i) + \frac{1}{2}\int_C F_u(\xi) H_0^{(2)}(\rho\xi)\, d\xi \tag{16}$$

$$W = -\frac{1}{2}\sum_{i} 2\pi j R_w(\xi_i) H_0^{(2)}(\rho\xi_i) + \frac{1}{2}\int_C F_w(\xi) H_0^{(2)}(\rho\xi)\, d\xi \tag{17}$$

where $R_{u,w}$ are the residues of $F_{u,w}$ in (4) and (5) at $\xi = \xi_i$ (surface wave poles) [4], [7]. The integral around the branch cut can be transformed to a real-axis integral by introducing the change of variable

$$\tau = \sqrt{k_0^2 - \xi^2} \qquad d\xi = \frac{-\tau\, d\tau}{\sqrt{k_0^2 - \tau^2}} \tag{18}$$

to give

$$I_u = \frac{1}{2}\int_{-\infty}^{\infty} \frac{\tau}{D_e(\tau)} H_0^{(2)}\left(\rho\sqrt{k_0^2 - \tau^2}\right) d\tau \tag{19}$$

$$I_w = \frac{1}{2}\int_{-\infty}^{\infty} \frac{\tau^2 H_0^{(2)}\left(\rho\sqrt{k_0^2 - \tau^2}\right)}{D_e(\tau)\cdot D_m(\tau)}. \tag{20}$$

Now consider the general integral

$$I = \frac{1}{2}\int_{-\infty}^{\infty} F(\tau) H_0^{(2)}\left(\rho\sqrt{k_0^2 - \tau^2}\right) d\tau \tag{21}$$

which can be written in a more convenient form, using the change of variable $\tau = k_0\eta$, as

$$I = \frac{k_0}{2}\int_{-\infty}^{\infty} F(k_0\eta) H_0^{(2)}\left(k_0\rho\sqrt{1-\eta^2}\right) d\eta. \tag{22}$$

For $k_0\rho$ large, we can use the large-argument form of the Hankel function:

$$I \sim \frac{k_0}{2}\sqrt{\frac{2}{\pi k_0\rho}}\, e^{j\pi/4}\int_{-\infty}^{\infty} \frac{F(k_0\eta)}{[1-\eta^2]^{1/4}} e^{-jk_0\rho\sqrt{1-\eta^2}}\, d\eta. \tag{23}$$

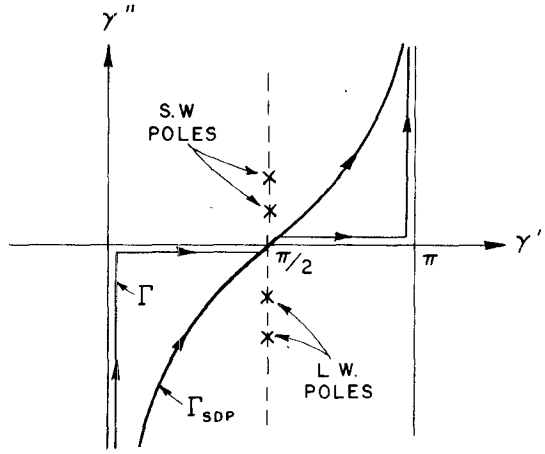

Fig. 3 Topology in the γ plane, showing the original path Γ and the steepest descent path Γ_{SDP}. The position of proper and improper surface wave poles (lossless case) is also shown.

Although the saddle point and the steepest descent path (SDP) can be found directly in the complex η plane, it is more convenient to perform the angular spectrum mapping:

$$\eta = \cos\gamma \qquad d\eta = -\sin\gamma\, d\gamma. \tag{24}$$

Then, (23) becomes

$$I \sim \frac{k_0}{2}\sqrt{\frac{2}{\pi k_0\rho}}\, e^{j\pi/4}\int_{\Gamma} F(k_0\cos\gamma)\sqrt{\sin\gamma}\, e^{-jk_0\rho\sin\gamma}\, d\gamma. \tag{25}$$

The exponential of (25) exhibits a saddle point at $\gamma = \pi/2$. The original path Γ and the SDP, denoted by Γ_{SDP}, are shown in Fig. 3. Also, Fig. 3 shows the position of the proper and improper surface wave poles for the lossless case (see [7]). As can be seen, the deformation of the original path Γ into Γ_{SDP} will never capture any of these poles. No other poles are assumed to be captured in the path deformation.

A conventional asymptotic evaluation of (25) can be carried out via the transformation

$$\sin\gamma = 1 - js^2 \qquad \cos\gamma = -s\sqrt{s^2 + 2j}$$
$$d\gamma = \frac{2j}{\sqrt{s^2 + 2j}}\, ds. \tag{26}$$

Now, (25) can be expressed in the complex s plane as

$$I \sim \frac{k_0}{2}\sqrt{\frac{2}{\pi k_0\rho}}\, e^{j\pi/4} e^{-jk_0\rho}\int_{-\infty}^{\infty} G(s)\, e^{-k_0\rho s^2}\, ds \tag{27}$$

where

$$G(s) = F\left(-k_0 s\sqrt{s^2 + 2j}\right)\sqrt{1 - js^2}\,\frac{2j}{\sqrt{s^2 + 2j}}. \tag{28}$$

A second-order asymptotic evaluation [8], [9] of (27) will give the following result, provided $G(0) = 0$ (which is the

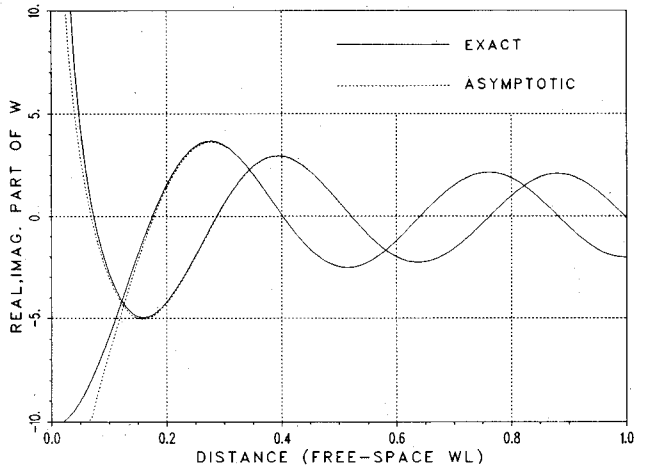

Fig. 4. Comparison between the exact W (numerical integration, (13)) and its asymptotic approximation (29) for $\epsilon_r = 12.8$, $d = 0.12\lambda_0$.

case for both U and W):

$$I \sim \frac{k_0}{2} I_0 \left[\sum_i \frac{R(b_i)}{b_i \sqrt{2j}} \left[1 - F\left(jk_0 \rho b_i^2 \right) \right] + \frac{1}{2k_0\rho} \left\{ \frac{G''(0)}{2\sqrt{2j}} + \sum_i \frac{R(b_i)}{b_i^3 \sqrt{2j}} \right\} \right] \quad (29)$$

where

$$I_0 = 2j \frac{e^{-jk_0\rho}}{k_0\rho} \quad (30)$$

$$b_i = \pm e^{j\pi/4} \sqrt{\frac{\xi_i}{k_0} - 1} \qquad \begin{pmatrix} + \text{for proper surface wave poles} \\ - \text{for improper surface wave poles} \end{pmatrix} \quad (31)$$

and $G''(0)$ is the second-order derivative of $G(s)$ in the s plane, evaluated at $s = 0$. Doing this for U and W, one obtains

$$G_u''(0) = 4j\sqrt{2j} \frac{1}{Y_0^2} \qquad Y_0 = \frac{\sqrt{\epsilon_r - 1}}{tg\left[k_0 d \sqrt{\epsilon_r - 1} \right]} \quad (32)$$

$$G_w''(0) = 4j\sqrt{2j} \frac{\epsilon_r}{\epsilon_r - 1}. \quad (33)$$

$R(b_i)$ in (29) are the residues of (28) at $s = b_i$. These residues can be easily related to those of the ξ plane at $\xi = \xi_i$ by

$$R(b_i) = \frac{R(\xi_i)}{\sqrt{k_0 \xi_i}}. \quad (34)$$

Finally, $F(x)$ in (29) is the transition function (defined in the Appendix). Fig. 4 shows a comparison between the numerical evaluation (13) and the asymptotic representation (29) for the case $\epsilon_r = 12.8$ and $d = 0.12\lambda_0$ when the source and field points are separated laterally along the dielectric–air interface. In the asymptotic evaluation, two proper and two improper surface wave poles are considered [7]. As can be seen, the asymptotic formula provides excellent results, even for source and field point separation distances as small as two tenths of a wavelength (λ_0). Although the comparison is not as good in all the cases, it can be said that the lateral source and field point separations for which the asymptotic solution begins to fail range typically between 0.2 and 1 wavelength. It should be mentioned that the above asymptotic result differs slightly from the one given in [4], where the poles of F in (22) are extracted in the η plane, and the resulting regular function is integrated up to the second-order term in closed form. The remaining integrals over the singularities are then approximated by their first-order terms. The difference between this approach and (29) arises in the second-order term of the asymptotic result, so the numerical difference between the two formulations is irrelevant in most cases, although (29) has been preferred here for simplicity.

III. Calculation of the Propagation Constant of an Infinite Microstrip Line

The first "full-wave" analysis of an infinite open microstrip line was reported by Denlinger [10]. By enforcing the boundary conditions in the spectral domain, he formulated the problem in terms of a pair of coupled integral equations, using a PWS integral representation for the fields. To simplify the solution to those equations he considered only electrically narrow strips, thus neglecting the transverse component of the current and assuming a known analytic variation of the longitudinal component along the transverse direction. Itoh and Mittra [11] numerically solved Denlinger's equations in the spectral domain, expanding both current components over a set of basis functions and applying Galerkin's method to obtain a matrix equation. Later, Farrar and Adams [12] and Jansen [13] extended the analysis to higher order modes and coupled microstrip lines. Recently, Kobayashi and Ando [14] presented a simplified spectral-domain formulation by using closed-form expressions for the longitudinal and transverse current distributions. Katehi and Alexopoulos [15] used the Sommerfeld integral representation for the grounded dielectric slab Green's function to compute the propagation constant of electrically narrow lines. They expanded the current along the longitudinal direction and applied Galerkin's method, assuming a known analytic variation of the current in the transverse direction.

Since the main purpose of this paper is to show the usefulness of the closed-form asymptotic representation for the Green's function, we have also restricted our attention to electrically narrow strips. This simplifies the formulation to only one current component. Also, a known analytic variation of this current along the transverse direction will be assumed.

The boundary condition is enforced in the spatial domain, and the Green's function is expressed in terms of Sommerfeld-type integrals. These integrals are evaluated using the numerical method described in subsection II-A when the distance between source and observation points is small, but the closed-form asymptotic expressions of

(29) are employed when the separation becomes larger. Since the spatial formulation requires an integration over the infinite length of the strip, the availability of a closed-form expression not only saves computer time, but also allows analytic integration when the current element is far enough. Both facts make possible a very efficient spatial-domain solution.

A. The Boundary Condition

Consider an infinite microstrip line (Fig. 1a) in which the current is flowing in the $\hat{y}$ direction. For electrically narrow strips and the fundamental mode it can be assumed that the $\hat{x}$ component of that current is negligible, so the current vector may be written in the form

$$\vec{J}(x, y) = F(x)\, e^{-jk_e y}\hat{y} \tag{35}$$

where $F(x)$ is the function describing the variation of the current density along the x direction, and k_e is the propagation constant of the mode. Furthermore, $F(x) = F(-x)$ via symmetry conditions fulfilled by $F(x)$. A widely used form of $F(x)$ which enforces the edge condition is

$$F^M(x) = \begin{cases} \dfrac{1}{\sqrt{w^2 - x^2}}, & |x| \leqslant w \\ 0, & \text{otherwise.} \end{cases} \tag{36}$$

This distribution was first proposed by Denlinger [10], who referred to it as Maxwell's function, because it was derived by Maxwell for the charge density distribution on an isolated conducting strip.

It is clear that the tangential electric field produced by J in (35) must vanish at any point on the metallic strip. This field can be written as

$$E_y(k_e, x, y) = \int_{-w}^{w}\int_{-\infty}^{\infty} F(x')\, e^{-jk_e y'} G_{yy}(x, y, x', y')\, dx'\, dy' = 0, \quad x, y \in \text{strip} \tag{37}$$

where G_{yy} represents the $\hat{y}$-directed electric field at (x, y) due to a $\hat{y}$-directed electric dipole of unit strength placed at (x', y'). The above equation is of the form $\mathcal{F}(k_e) = 0$, where $\mathcal{F}$ is the operator in (37). Such an equation can be solved using simple search techniques, such as the interval halving method or Newton's method.

Equation (37) admits further simplification if the point (x, y) selected to enforce the boundary condition is the center of the strip (0,0). In that case, the symmetry of the problem and the oddness of the imaginary part of the exponential reduce (37) to

$$\int_0^w F(x') \int_{-\infty}^{\infty} G_{yy}(x', y') \cos(k_e y')\, dx'\, dy' = 0. \tag{38}$$

This equation will be the basis of our calculations and will be referred to as the boundary condition in the spatial domain.

B. Field Calculation

From (1) and (38) the $\hat{y}$-directed electric field at the origin can be written as

$$E_y(k_e, 0, 0) \propto \int_0^w F(x') I(k_e, x')\, dx' \tag{39}$$

with

$$I(k_e, x') = \int_0^{\infty} \left\{ k_0^2 U + \frac{\partial^2}{\partial y^2}\left[U - \frac{\epsilon_r - 1}{\epsilon_r} W \right] \right\} \cdot \cos(k_e y')\, dy'. \tag{40}$$

The second derivative before the brackets can be removed using integration by parts to give

$$I(k_e, x') = k_0^2 \int_0^{\infty} U \cos(k_e y')\, dy' - k_e^2 \int_0^{\infty} \left\{ U - \frac{\epsilon_r - 1}{\epsilon_r} W \right\} \cos(k_e y')\, dy' \tag{41}$$

where use has been made of the following (from (2)–(7)):

$$\frac{\partial G}{\partial y} = -\frac{\partial G}{\partial y'} \tag{42a}$$

$$\lim_{y' \to \infty} G(x, y, x', y') = 0 \tag{42b}$$

$$\lim_{y' \to \infty} \frac{\partial}{\partial y'} G(x, y, x', y') = 0 \tag{42c}$$

$$\lim_{(y - y') \to 0} \frac{\partial}{\partial y'} G(x, y, x', y') = 0 \tag{42d}$$

where G represents either U or W. Now the problem has been reduced to that of computing two integrals of the form

$$I^G(k_e, x') = \int_0^{\infty} G \cos(k_e y')\, dy' \tag{43}$$

where G again represents U or W.

From (12) and (13) we know that G has a singularity of the type $1/\rho$:

$$G = \frac{F^{\infty}}{\rho} + G' \tag{44}$$

where G' represents the nonsingular part of G.

Such a singularity can be integrated analytically to give

$$\int_0^{\infty} \frac{F^{\infty}}{\sqrt{x'^2 + y'^2}} \cos(k_e y')\, dy' = F^{\infty} K_0(k_e x') \tag{45}$$

where K_0 is the zero-order modified Bessel function.

Finally we have

$$I^G(k_e, x') = F^{\infty} K_0(k_e x') + \int_0^{\infty} G' \cos(k_e y')\, dy'. \tag{46}$$

The integral on the right-hand side of (46) can be calculated numerically, since G' does not contain any singularity. This numerical integration is terminated at certain y'_L for which the integrals in (16) and (17) become negligible. From such region to infinity only surface waves exist, and

their contribution can be evaluated analytically. In most cases, y'_L ranges from five to ten free-space wavelengths. The value of G' in (46) is calculated numerically only for small distances between source and field points, but the efficient closed-form asymptotic representation is used along most of the range of integration.

Going back to (39), the field can then be calculated as

$$E_y(k_e,0,0) \propto (k_0^2 - k_e^2)\left\{ F_u^{\infty} \int_0^w F(x') K_0(k_e x')\, dx' + \int_0^w F(x') \int_0^{\infty} U' \cos(k_e y')\, dy' \right\} + k_e^2 \left(\frac{\epsilon_r - 1}{\epsilon_r} \right) \left\{ F_w^{\infty} \int_0^w F(x') K_0(k_e x')\, dx' + \int_0^w F(x') \int_0^{\infty} W' \cos(k_e y')\, dy' \right\}. \quad (47)$$

The first integral between braces can again be evaluated analytically for $F(x')$ of the form (36) as [16]

$$\int_0^w \frac{K_0(k_e x')}{\sqrt{w^2 - x'^2}}\, dx' = \frac{\pi}{2} I_0\left(\frac{k_e w}{2}\right) K_0\left(\frac{k_e w}{2}\right). \quad (48)$$

To evaluate the second integral, we first note that the functions

$$I^{G'}(k_e, x') = \int_0^{\infty} G' \cos(k_e y')\, dy' \quad (49)$$

have a quite smooth variation with x' for small x', which is precisely the case for electrically narrow lines. It follows that these functions can be very accurately approximated by an nth-order polynomial, namely

$$I^{G'}(k_e, x') \simeq A_0 + A_1 x' + \cdots + A_n x'^n \quad (50)$$

with the advantage that $F^M(x') \cdot I^{G'}(k_e x')$ can be integrated on x' in closed form [16]:

$$\int_0^w \frac{x'^{2n+1}}{\sqrt{w^2 - x'^2}}\, dx' = \frac{2n!!}{(2n+1)!!} w^{2n+1} \quad (51)$$

$$\int_0^w \frac{x'^{2n+1}}{\sqrt{w^2 - x'^2}}\, dx' = \frac{(2n-1)!!}{(2n)!!} \frac{\pi}{2} w^{2n} \quad (52)$$

where $(2n)!! = 2 \cdot 4 \cdots (2n)$, and $(2n+1)!! = 1 \cdot 3 \cdots (2n+1)$.

Fig. 5 shows the behavior of $I^{U'}$ corresponding to the case of Fig. 4 and its second-order polynomial approximation (if the order of the polynomial is increased to four, the value of the integral over x' differs less than 0.1 percent from the second-order polynomial value).

So finally, (47) can be written as

$$E_y(k_e,0,0) \propto (k_0^2 - k_e^2)\left\{ F_u^{\infty} \frac{\pi}{2} I_0\left(\frac{k_e w}{2}\right) K_0\left(\frac{k_e w}{2}\right) + A_0^u \frac{\pi}{2} + A_1^u w + A_2^u w^2 \frac{\pi}{2} \right\} + k_e^2 \left(\frac{\epsilon_r - 1}{\epsilon_r} \right) \left\{ F_w^{\infty} \frac{\pi}{2} I_0\left(\frac{k_e w}{2}\right) K_0\left(\frac{k_e w}{2}\right) + A_0^w \frac{\pi}{2} + A_1^w + A_2^w w^2 \frac{\pi}{2} \right\}. \quad (53)$$

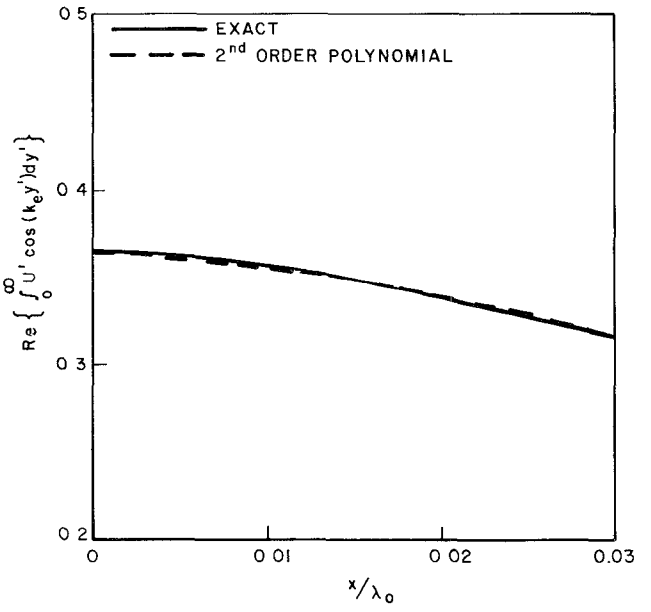

Fig. 5. Variation of the integral (49) as a function of x' for the case of Fig. 4 and its second-order polynomial approximation ($k_e = 3k_0$).

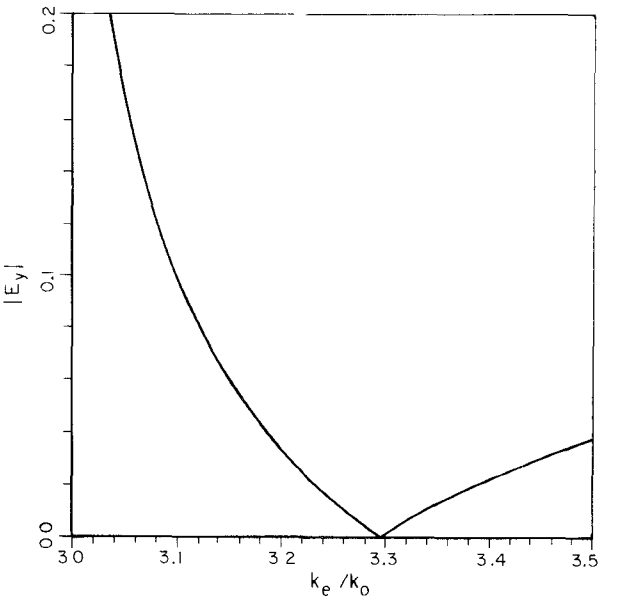

Fig. 6. Typical variation of the tangential electric field on the center of the strip as a function of the propagation constant k_e. The zero field boundary condition is satisfied at $k_e = k_0\sqrt{\epsilon_{r_{\text{eff}}}}$ ($\epsilon_r = 12.8$, $d = 0.12\lambda_0$, $2w = 0.06\lambda_0$).

Now a plot of $|E_y|$ versus k_e/k_0 should exhibit a zero at that $k_e = k_0\sqrt{\epsilon_{r_{\text{eff}}}}$ corresponding to the mode actually propagating in the transmission line. Fig. 6 shows typical results.

To automatically find $\sqrt{\epsilon_{r_{\text{eff}}}}$, a Newton–Raphson search procedure can be implemented in the equation

$$\text{Re}\{E_y(k_e,0,0)\} = 0. \quad (54)$$

Using the quasi-static value of $\sqrt{\epsilon_{r_{\text{eff}}}}$ or simply $\sqrt{\epsilon_r}$ as the starting point, the final value is found in only a few iterations (normally two to four).

IV. Moment Method Solution for the Input Impedance of a Center-Fed Printed Strip Dipole

The printed dipole was first treated with an assumed sinusoidal current distribution by Tsandoulas [17] and Uzunoglu *et al.* [18]; later Rana and Alexopoulos [19] introduced the moment method (MM) solution for the center-fed printed dipole by expanding the unknown current of the dipole by piecewise-sinusoidal (PS) basis functions. This work was then extended to different geometries by Katehi and Alexopoulos [20], [21]. It is noted that the MM solution of such geometries is very time consuming because the grounded dielectric slab Green's function involved in the formulation is very poorly convergent, as mentioned earlier.

In the following, an efficient MM calculation of the input impedance for the printed strip dipole shown in Fig. 1(b) will be discussed. The printed strip dipole considered here is center-fed by a delta gap generator and has the length L and the width $2w$. The unknown longitudinal current on the strip has been expanded by N overlapping PS basis functions. The transversal current variation is chosen such that the current satisfies the edge condition [3], [21] and is in the form of (36).

The MM matrix equation is then formulated as

$$\underset{N\times N}{[Z_{mn}]}\underset{N\times 1}{[I_n]} = \underset{N\times 1}{[V_n]} \tag{55}$$

where Z_{mn} is the reaction between the test function n and the basis function m; the I_n's are unknown coefficients of the basis functions which ought to be determined from the above matrix equation and the V_n's are excitations. For the center-fed delta gap generator type excitation, the input impedance of the printed strip dipole Z_{in} is numerically given by

$$Z_{\text{in}} = \frac{1}{I(0)} \tag{56}$$

where $I(0)$ is the value of the current at the center of the strip dipole.

The efficient evaluation of Z_{mn} is the key to an efficient MM solution for the input impedance of the printed strip dipole. In the following such efficient formulation of Z_{mn} will be presented. It is recalled that Z_{mn} can be written as [3]

$$Z_{mn} = \int_{y_n-a}^{y_n+a}\int_{-w}^{w}\int_{y_m-a}^{y_m+a}\int_{-w}^{w} J_n^T(x', y') \cdot G_{yy} \cdot J_m(x, y)\, dx'\, dy'\, dx\, dy \tag{57}$$

where G_{yy} is the $\hat{y}\hat{y}$ component of the microstrip dyadic Green's function and was given in (1); $J_m(x, y)$ and $J_n^T(x', y')$ are the basis and testing functions, respectively, and are given by

$$J_m(x, y) = \frac{1}{\pi\sqrt{w^2 - x^2}} \frac{\sin k_e(a - |y - y_m|)}{\sin k_e a}, \qquad |y - y_m| < a \tag{58a}$$

and

$$J_n^T(x', y') = \delta(x') \frac{\sin k_e(a - |y' - y_n|)}{\sin k_e a}, \qquad |y' - y_n| < a \tag{58b}$$

where $(2w)$ is the width of the strip

$$\left(a = |y_{m+1} - y_m| = \frac{L}{N+1}\right)$$

and k_e is the effective wavenumber of the PS basis function. After incorporating (58a), (58b), and (1) into (57), using integration by parts, and performing the integration along x', one will get

$$\begin{aligned} Z_{nm} = {} & \frac{1}{2\pi\omega\epsilon_0} \frac{1}{(\sin k_e a)^2} \int_0^w \frac{2}{\pi\sqrt{w^2 - x^2}} \int_{y_n-a}^{y_n+a} \Big\{ k_e[P(y_m + a) + P(y_m - a) \\ & - 2\cos(k_e a) P(y_m)] - k_e^2 \cdot \Big[\int_{y_m-a}^{y_m} [Q] \sin(k_e(y - y_m - a))\, dy \\ & + \int_{y_m}^{y_m+a} [Q] \sin(k_e(y_m + a - y))\, dy \Big] \Big\} \\ & \cdot \sin(k_e(a - |y' - y_n|))\, dy'\, dx \end{aligned} \tag{59}$$

where

$$P = U - \frac{\epsilon_r - 1}{\epsilon_r} W \tag{60a}$$

$$Q = \left(1 - \frac{k_0^2}{k_e^2}\right) U - \frac{\epsilon_r - 1}{\epsilon_r} W \tag{60b}$$

and the efficient representations of U and W for small and large lateral separations are given in (12), (13), and (29), respectively. Note that if $k_e = k_0$, Q is given by W multiplied by a constant.

The double integrals of y and y' variables in (59) can be transformed to a single integral via a rotation of coordinate system [3], i.e.,

$$u = \frac{1}{\sqrt{2}}(y' + y) \qquad v = \frac{1}{\sqrt{2}}(y' - y) \qquad dy'\, dy = du\, dv \tag{61a}$$

$$\begin{aligned} & \int_{y_{1n}}^{y_{2n}} \int_{y_{1m}}^{y_{2m}} Q((y' + y), (y' - y))\, dy'\, dy \\ & = \int_{v_0}^{v_2} \int_{v+\sqrt{2}y_{1n}}^{-v+\sqrt{2}y_{2m}} Q(u, v)\, du\, dv \\ & \quad + \int_{v_1}^{v_0} \int_{-v+\sqrt{2}y_{1m}}^{v+\sqrt{2}y_{2n}} Q(u, v)\, du\, dv \end{aligned} \tag{61b}$$

where

$$v_2 = \frac{1}{\sqrt{2}}(y_{2m} - y_{1n}) \qquad v_1 = \frac{1}{\sqrt{2}}(y_{1m} - y_{2n})$$

$$v_0 = \frac{1}{\sqrt{2}}(y_{1m} - y_{1n}). \tag{61c}$$

The u dependence can now be integrated analytically. After normalizing the integral of the v variable between 0 and 1 by changing the variation to α, the final result will be given by

$$Z_{mn} = \frac{1}{2\pi\omega\epsilon_0}\frac{k_e a}{(\sin k_e a)^2}\int_0^w \frac{2}{\pi\sqrt{w^2 - x^2}} \cdot \left\{ \int_0^1 [P_1 + P_2 + P_3 + P_4 - 2\cos(k_e a)(P_5 + P_6)] \cdot \sin(k_e a(1-\alpha))\, d\alpha - 2k_e a \cdot \left[\int_0^{0.5} [Q_1 + Q_2][S_1]\, d\alpha + \int_{0.5}^{1.0} [Q_1 + Q_2][S_2]\, d\alpha \right] \right\} dx \tag{62}$$

where

$$P_{1-4} = P|_{\rho = \sqrt{x^2 + (y_{mn} \pm a(1 \pm \alpha))^2}}$$

$$P_{5,6} = P_{\rho = \sqrt{x^2 + (y_{mn} \pm a\alpha)^2}} \tag{63a}$$

$$Q_{1-2} = Q|_{\rho = \sqrt{x^2 + (y_{mn} \pm 2a\alpha)^2}} \tag{63b}$$

$$y_{mn} = |y_m - y_n| \tag{63c}$$

and P and Q are given in (60a) and (60b), respectively. Also

$$[S_1] = (1 - \alpha(2 + \cos(2k_e a))\cos(2k_e a\alpha) - \alpha\sin(2k_e a)\sin(2k_e a\alpha) + \frac{1}{2k_e a}[(2 + \cos(2k_e a))\sin(2k_e a\alpha) - \sin(2k_e a)\cos(2k_e a\alpha)] \tag{64}$$

$$[S_2] = -(1-\alpha)\cos(2k_e a(1-\alpha)) + \frac{1}{2k_e a}\sin(2k_e a(1-\alpha)). \tag{65}$$

It is noted that the formulation of Z_{mn} given in (59) is very efficient, particularly if P and Q are given in terms of the efficient closed-form representations of U and W. For the case when $m = n$ (the self term), finally $y_{mn} = 0$, as is evident from (63c); therefore from (63a) and (63b),

$$P_1 = P_2 \qquad P_3 = P_4 \qquad P_5 = P_6 \tag{66}$$

and

$$Q_1 = Q_2. \tag{67}$$

For the self term Z_{mm}, the numerical integration in the α domain can be efficiently improved if the singular behavior of P and Q (see (12) and (13)) along with the rest of the integrand in (62) is analytically integrated in the small interval from zero to δ_α for δ_α in the order of $0.1\ k_e a$. Note that for the small interval around the zero, $[S_1]$ in (64) and $\sin k_e a(1-\alpha)$ in (62) can be approximated by the two-term Taylor expansions

$$[S_1] \simeq 1 - \frac{\sin(2k_e a)}{2k_e a},$$

$$\sin k_e a(1-\alpha) \simeq \sin(k_e a) - (k_e a\alpha)\cos k_e a. \tag{68}$$

Use can also be made of the following identities:

$$\int \frac{d\alpha}{\sqrt{x^2 + (a\alpha)^2}} = \frac{1}{a}\ln\left(\alpha + \sqrt{\frac{x^2}{a^2} + \alpha^2}\right) \tag{69a}$$

and

$$\int \frac{\alpha\, d\alpha}{\sqrt{x^2 + (a\alpha)^2}}\, d\alpha = \frac{1}{a}\sqrt{\frac{x^2}{a^2} + \alpha^2}. \tag{69b}$$

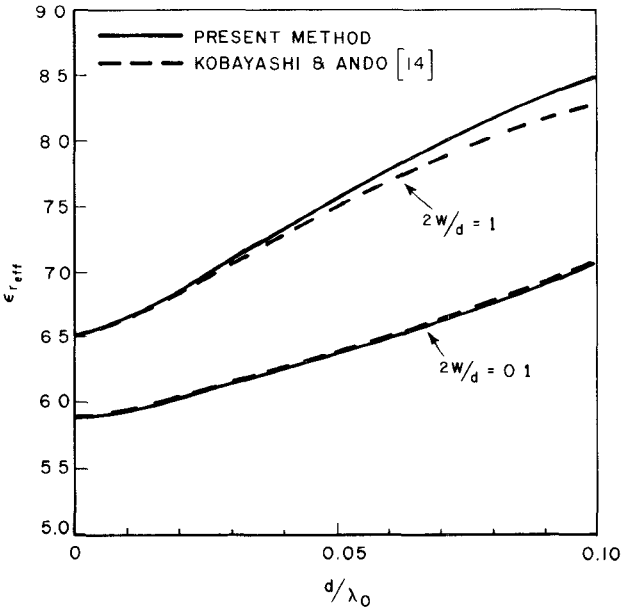

Fig. 7. Calculated effective dielectric constant as a function of substrate thickness ($\epsilon_r = 9.7$).

V. Results and Conclusions

Considering first the calculation of the effective dielectric constant of a microstrip line, Fig. 7 shows a comparison between results obtained using the approach described in Section III and those reported by Kobayashi and Ando [14]. In this case, the relative dielectric constant is assumed to be $\epsilon_r = 9.7$, and the effective dielectric constant is plotted as a function of d/λ_0, with $2w/d$ as a parameter, for $2w/d = 0.1$ and 1. As can be seen, the agreement is excellent for $2w/d = 0.1$, but a slight discrepancy (less than 2.5 percent in the worst case) arises in the curve corresponding to $2w/d = 1$. The reason for this is that the actual current distribution on the strip begins to differ from the Maxwell function when w increases. Closed-form expressions for the current distribution as a function of the aspect ratio $2w/d$ have been given by Kobayashi [22], and

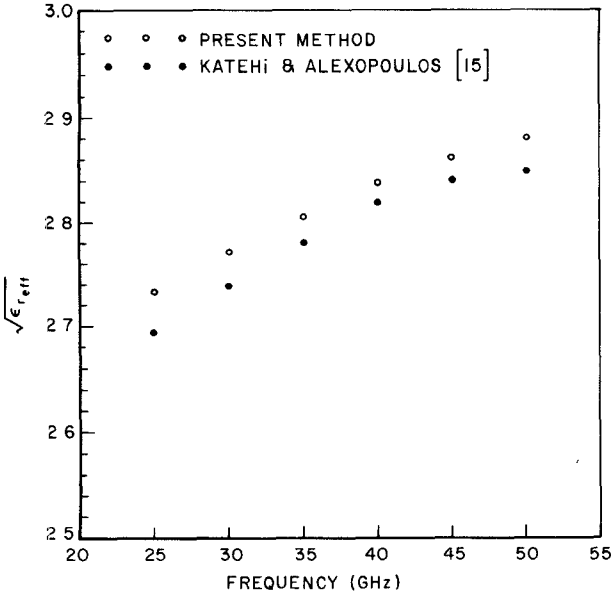

Fig. 8. Calculated effective dielectric constant as a function of frequency ($\epsilon_r = 9.6$, $2w = d = 0.6$ mm).

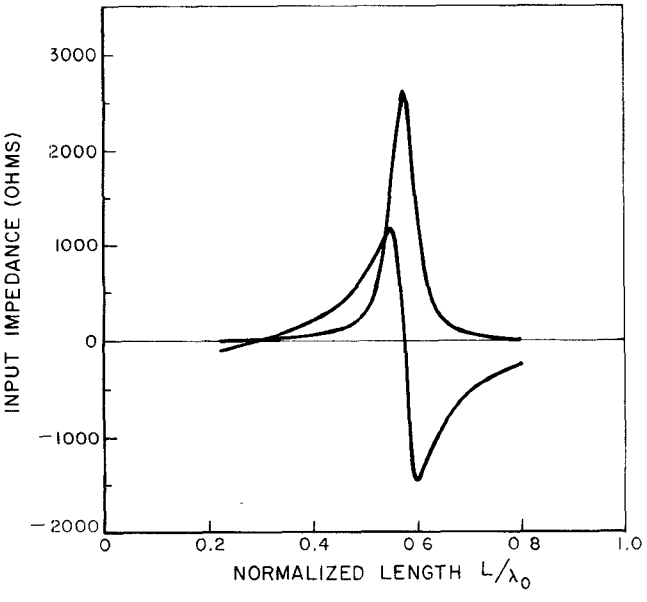

Fig. 9. Input impedance (real and imaginary parts) of the strip dipole versus normalized length L/λ_0. The strip width is $0.01\lambda_0$; dielectric constant $\epsilon_r = 3.25$ and dielectric thickness $d = 0.0796\lambda_0$.

can easily be incorporated into our formulation. Finally, Fig. 8 shows another comparison with results given by Katehi and Alexopoulos [15]. The dielectric constant is now 9.6, and the effective dielectric constant is plotted as a function of frequency for $2w = d = 0.6$ mm. The slight discrepancy (of the order of 1 percent) between the two results is attributed to the effective width w_e used in [15] to account for conductor thickness.

On the other hand, Fig. 9 shows the input impedance (real and imaginary parts) of the strip dipole of Fig. 1(b) versus normalized length (with respect to the free-space wavelength). The microstrip dipole antenna has a width of $0.01\lambda_0$. For dipoles with a length less than $0.2\lambda_0$, only a single PS mode is used, and for larger dipoles three expansion (PS) modes with an effective wavenumber ($k_e = k_0\sqrt{(\epsilon_r+1)/2}$) have been utilized. It is noted that the resonant length of the strip dipole is a function of substrate thickness and dielectric constant, and it is less than the resonant length of the strip dipole in free space. This is due to the fact that the presence of the substrate increases the effective electrical length of the strip dipole. Two resonance phenomena have been observed (which yield a purely real input impedance). The first is at $L \simeq 0.29\lambda_0$ and the second is at $L \simeq 0.58\lambda_0$, where L is the length of the dipole. The quantities $0.29\lambda_0$ and $0.58\lambda_0$ are the "effective" half and full wavelength of the air–dielectric substrate structure. It is also noted that the reactive part of the impedance is strongly dependent on the width of the strip. This can be seen by modeling the input impedance of the strip dipole as the mutual impedance between the two nearby filament currents over the grounded dielectric slab in which their lengths are equal to the length of the original strip dipole and their lateral separation is a function of its width [24]. In this configuration, the real part of the mutual impedance is almost constant; however, the reactive part is proportional to the logarithm of the inverse of the lateral separation. It is noted that for the calculation of the input impedance of Fig. 9, the efficient closed-form representations of U and W given in (29) were utilized over 30–40 percent of the time, which results in a significant savings in computational time for even such a small structure.

In conclusion, it has been shown how the efficient closed-form asymptotic representation of the grounded dielectric slab Green's function is incorporated into the solution of two canonical problems in microstrip circuit/antenna analysis. The advantages of these closed-form expressions are apparent: since they only involve relatively simple and well-known functions, their calculation is far more efficient than numerical integration, even when some analytical treatment is incorporated to speed up the convergence. On the other hand, they provide more physical insight since the asymptotic closed-form Green's function describes the field contributions as arising separately and explicitly from such phenomena as surface, leaky, and space waves. These features make the combination method of moments/asymptotic Green's function look very promising for analyzing microstrip structures.

Appendix
The Transition Function $F(x)$

The transition function $F(x)$ is defined in [23] as follows:

$$F(x) = 2j\sqrt{x}\, e^{jx}\int_{\sqrt{x}}^{\infty} e^{-jt^2}\, dt, \qquad -\frac{3\pi}{2} < \arg(x) < \frac{\pi}{2} \tag{A1}$$

where x can be complex. The branch cut definition of $\sqrt{x}$ in (A1) is chosen as defined in [9].

It can be shown that, with this definition of F,

$$\int_{-\infty}^{\infty} \frac{e^{-\Omega s^2}}{s-b}\,ds = -\frac{1}{b}\sqrt{\frac{\pi}{\Omega}}\,F\left(j\Omega b^2\right) = \pm 2j\sqrt{\pi}\,e^{-\Omega b^2}Q\left(\mp jb\sqrt{\Omega}\right), \qquad \operatorname{Im}(b) \gtrless 0 \tag{A2}$$

where Ω is a real positive number and b is complex in general. Q is the transition function defined in [8].

Since the proper and improper surface wave poles considered throughout the paper are such that in the s plane $b_i = \pm e^{j\pi/4}B_i$ (+ for pswp; − for iswp), B_i being a real positive number, (A1) can be expressed as

$$F\left(j\Omega b_i^2\right) = F\left(-\Omega B_i^2\right) = 2e^{-j\pi/4}\sqrt{\Omega}\,B_i\,e^{-j\Omega B_i^2} \cdot \left\{\frac{\sqrt{\pi}}{2} - e^{-j\pi/4}\sqrt{\frac{\pi}{2}}\left[C\left(\sqrt{\frac{2\Omega}{\pi}}\,B_i\right) + jS\left(\sqrt{\frac{2\Omega}{\pi}}\,B_i\right)\right]\right\} \tag{A3}$$

where $C(z)$ and $S(z)$ are Fresnel integrals, defined as

$$C(z) = \int_0^z \cos\left(\frac{\pi}{2}t^2\right)dt \qquad S(z) = \int_0^z \sin\left(\frac{\pi}{2}t^2\right)dt. \tag{A4}$$

It is also useful to note that, for Ωb_i^2 large,

$$F\left(j\Omega b_i^2\right) \sim 1 + \frac{1}{2\Omega b_i^2} + 0\left(\frac{1}{\Omega^2 b_i^4}\right). \tag{A5}$$

References

[1] D. M. Pozar, "Input impedance and mutual coupling of rectangular microstrip antennas," *IEEE Trans. Antennas Propagat.*, vol. AP-30, pp. 1191–1196, Nov. 1982.

[2] I. E. Rana and N. G. Alexopoulos, "Current distribution and input impedance of printed dipoles," *IEEE Trans. Antennas Propagat.*, vol. AP-29, pp. 99–105, Jan. 1981.

[3] S. Barkeshli, "An efficient approach for evaluating the planar microstrip Green's function and its applications to the analysis of microstrip antennas and arrays," Ph.D. dissertation, The Ohio State University, Dept. of Electrical Engineering, Columbus, OH, 1988.

[4] S. Barkeshli, P. H. Pathak, and M. Marin, "An asymptotic closed-form microstrip surface Green's function for the efficient moment method analysis of mutual coupling in microstrip antenna arrays," submitted to *IEEE Trans. Antennas Propagat.*

[5] J. R. Mosig and T. K. Sarkar, "Comparison of quasi-static and exact electromagnetic fields from the horizontal electric dipole above a lossy dielectric backed by an imperfect ground plane," *IEEE Trans. Microwave Theory Tech.*, vol. MTT-34, pp. 379–387, Apr. 1986.

[6] D. R. Jackson and N. G. Alexopoulos, "An asymptotic extraction technique for evaluating Sommerfeld-type integrals," *IEEE Trans. Antennas Propagat.*, vol. AP-34, Dec. 1986.

[7] M. Marin, S. Barkeshli, and P. H. Pathak, "On the location of proper and improper surface wave poles for the grounded dielectric slab," submitted to *IEEE Trans. Antennas Propagat.*

[8] L. B. Felsen and N. Marcuvitz, *Radiation and Scattering of Waves*. Englewood Cliffs, NJ: Prentice-Hall, 1973.

[9] R. G. Rojas, "Comparison between two asymptotic methods," *IEEE Trans. Antennas Propagat.*, vol. AP-35, pp. 1489–1492, Dec. 1987.

[10] E. J. Denlinger, "A frequency dependent solution for microstrip transmission lines," *IEEE Trans. Microwave Theory Tech.*, vol. MTT-19, pp. 30–39, Jan. 1971.

[11] T. Itoh and R. Mittra, "Spectral-domain approach for calculating the dispersion characteristics of microstrip lines," *IEEE Trans. Microwave Theory Tech.*, vol. MTT-21, pp. 496–499, July 1973.

[12] A. Farrar and A. T. Adams, "Computation of propagation constants for the fundamental and higher order modes in microstrip," *IEEE Trans. Microwave Theory Tech.*, vol. MTT-24, pp. 456–460, July 1976.

[13] R. H. Jansen, "High-speed computation of single and coupled microstrip parameters including dispersion, high-order modes, loss and finite strip thickness," *IEEE Trans. Microwave Theory Tech.*, vol. MTT-26, pp. 75–82, Feb. 1978.

[14] M. Kobayashi and F. Ando, "Dispersion characteristics of open microstrip lines," *IEEE Trans. Microwave Theory Tech.*, vol. MTT-35, pp. 101–105, Feb. 1987.

[15] P. B. Katehi and N. G. Alexopoulos, "Frequency-dependent characteristics of microstrip discontinuities in millimeter-wave integrated circuits," *IEEE Trans. Microwave Theory Tech.*, vol. MTT-33, pp. 1029–1035, Oct. 1985.

[16] I. S. Gradshteyn and I. M. Ryzhik, *Table of Integrals, Series, and Products*. New York: Academic Press, 1980.

[17] G. N. Tsandoulas, "Excitation of a grounded dielectric slab by a horizontal dipole," *IEEE Trans. Antennas Propagat.*, vol. AP-17, pp. 156–161, Mar. 1969.

[18] N. K. Uzunoglu, N. G. Alexopoulos, and J. G. Fikioris, "Radiation properties of microstrip dipoles," *IEEE Trans. Antennas Propagat.*, vol. AP-27, pp. 853–858, Nov. 1979.

[19] N. G. Alexopoulos and I. E. Rana, "Mutual impedance computation between printed dipoles," *IEEE Trans. Antennas Propagat.*, vol. AP-29, pp. 106–111, Jan. 1981.

[20] P. B. Katehi and N. G. Alexopoulos, "On the effect of substrate thickness and permittivity on printed circuit dipole properties," *IEEE Trans. Antennas Propagat.*, vol. AP-39, pp. 34–39, Jan. 1983.

[21] P. B. Katehi and N. G. Alexopoulos, "On the modeling of electromagnetically coupled microstrip antennas—The printed strip dipole," *IEEE Trans. Antennas Propagat.*, vol. AP-32, pp. 1179–1186, Nov. 1984.

[22] M. Kobayashi, "Longitudinal and transverse current distributions on microstriplines and their closed-form expression," *IEEE Trans. Microwave Theory Tech.*, vol. MTT-33, pp. 794–788, Sept. 1985.

[23] R. G. Kouyoumjian and P. H. Pathak, "A uniform geometrical theory of diffraction for an edge in a perfectly conducting surface," *Proc. IEEE*, vol. 62, pp. 1448–1461, 1974.

[24] E. H. Newman, "The equivalent separation(s) for the self-impedance of thin strips," *IEEE Trans. Antennas Propagat.*, vol. AP-35, Jan. 1987.

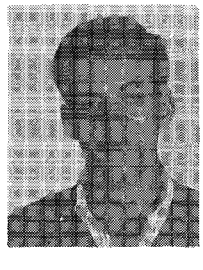

Miguel Marin (M'87) was born in Madrid, Spain, on June 14, 1960. He received the M.S. and Ph.D. degrees in electrical engineering from the Polytechnic University of Madrid in 1983 and 1987, respectively.

From 1983 to 1987 he was with the Department of Radiation, Polytechnic University of Madrid, as a Teaching Assistant in Electromagnetics. Since 1987 he has been a Fulbright Fellow at the Ohio State University ElectroScience Laboratory. His present research interests in-

clude numerical and asymptotic techniques for the modeling of printed circuit antennas and components.

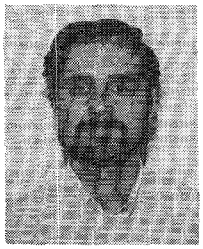

Sina Barkeshli was born in Tehran, Iran, on July 30, 1956. He received the B.S.E.E. and M.S.E.E. degrees from the University of Kansas in 1979 and 1982, respectively, and the Ph.D. degree in electrical engineering from Ohio State University in 1988.

From 1980 to 1982 he was with the Remote Sensing Laboratory of the University of Kansas as a graduate research associate. From 1982 until 1988 he worked as a graduate research associate at the Ohio State University Electroscience Laboratory. Currently he holds the position of senior research analyst at Sabbagh Associate Inc. His interests are primarily focused on the interaction of electromagnetic waves with layered media, microstrip antennas, and millimeter-wave integrated circuit elements, as well as high-frequency asymptotic techniques.

Dr. Barkeshli is a member of Sigma Xi and Eta Kappa Nu.

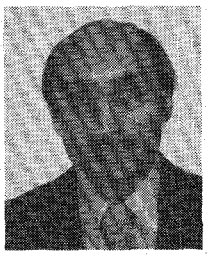

Prabhakar H. Pathak (M'76–SM'81–F'86) received the B.Sc. degree in physics from the University of Bombay, India, in 1962, the B.S. degree in electrical engineering from Louisiana State University, Baton Rouge, in 1965, and the M.S. and Ph.D. degrees in electrical engineering from Ohio State University, Columbus, in 1970 and 1973, respectively.

From 1965 to 1966 he was an instructor in the Department of Electrical Engineering at the University of Mississippi, Oxford. During the summer of 1966, he worked as an electronics engineer with the Boeing Company in Renton, WA. Since 1968 he has been with the Ohio State University ElectroScience Laboratory, where his research interests have centered on mathematical methods, electromagnetic antenna and scattering problems, and uniform ray techniques. He is also an Associate Professor in the Department of Electrical Engineering at Ohio State University, where he teaches courses in electromagnetics, antennas, and linear systems.

Dr. Pathak has participated in invited lectures and in several short courses on the uniform geometrical theory of diffraction, both in the United States and abroad. He has also authored and coauthored chapters on ray methods for five books. Dr. Pathak is a member of Commission B of the International Scientific Ratio Union (URSI), and of Sigma Xi.